Trace elements during primordial plexiform network formation in human cerebral organoids

Rafaela C Sartore [1, 2] , **Simone C Cardoso** [3] , **Yury V Lages** [1, 2] , **Julia M Paraguassu** [1, 2] , **Rodrigo F Madeiro da Costa** [1] , **Marilia Z Guimaraes** [1, 2] , **Carlos A Pérez** [4] , **Stevens K Rehen** Corresp. [1, 5]

[1] Instituto D'Or de Pesquisa e Ensino, Rio de Janeiro, RJ, Brazil

[2] Instituto de Ciências Biomédicas, Universidade Federal do Rio de Janeiro, Rio de Janeiro, RJ, Brazil

[3] Instituto de Física, Universidade Federal do Rio de Janeiro, Rio de Janeiro, RJ, Brazil

[4] Laboratório Nacional de Luz Síncroton, Campinas, SP, Brazil

[5] Instituto de Ciências Biomédicas, Universidade Federal do Rio de Janeiro, Rio de Janeiro, Brazil

Corresponding Author: Stevens K Rehen
Email address: srehen@lance-ufrj.org

Systematic studies of micronutrients during brain formation are hindered by restrictions to animal models and adult post-mortem tissues. Recently, advances in stem cell biology have enabled recapitulation of the early stages of human telencephalon development in vitro. In the present work, we exposed cerebral organoids derived from human pluripotent stem cells to synchrotron radiation in order to measure how biologically valuable micronutrients are incorporated and distributed in the exogenously developing brain. Our findings indicate that elemental inclusion in organoids is consistent with human brain tissue and involves calcium, iron, phosphorus, potassium, sulfur, and zinc. Local trends in concentrations suggest a switch from passive to actively mediated transport across cell membranes. Finally, correlational analysis for pairs of elements shows spatially conserved patterns, suggesting they may physically associate, be stored in similar compartments or used in related biological processes. These findings might reflect which trace elements are important during human brain development and will support studies aimed to unravel the consequences of disrupted metal homeostasis for neurodevelopmental diseases, including those manifested in adulthood.

Trace elements during primordial plexiform network formation in human cerebral organoids

Rafaela C. Sartore[1,2], Simone C. Cardoso[3], Yury V. Lages[1,2], Julia M. Paraguassu[1,2], Rodrigo F. Madeiro da Costa[1], Marilia Z.P. Guimarães[2], Carlos A. Pérez[4], Stevens K. Rehen[1,2*]

[1]D'Or Institute for Research and Education (IDOR) · Rio de Janeiro · Brazil
[2]Institute of Biomedical Sciences · Federal University of Rio de Janeiro · Brazil
[3]Physics Institute · Federal University of Rio de Janeiro · Brazil
[4]Brazilian Synchrotron Light Laboratory · São Paulo · Brazil

* Corresponding Author: Stevens Rehen

Email: srehen@lance-ufrj.org

Abstract

Systematic studies of micronutrients during brain formation are hindered by restrictions to animal models and adult post-mortem tissues. Recently, advances in stem cell biology have enabled recapitulation of the early stages of human telencephalon development in vitro. In the present work, we exposed cerebral organoids derived from human pluripotent stem cells to synchrotron radiation in order to measure how biologically valuable micronutrients are incorporated and distributed in the exogenously developing brain. Our findings indicate that elemental inclusion in organoids is consistent with human brain tissue and involves calcium, iron, phosphorus, potassium, sulfur, and zinc. Local trends in concentrations suggest a switch from passive to actively mediated transport across cell membranes. Finally, correlational analysis for pairs of elements shows spatially conserved patterns, suggesting they may physically associate, be stored in similar compartments or used in related biological processes. These findings might reflect which trace elements are important during human brain development and will support studies aimed to unravel the consequences of disrupted metal homeostasis for neurodevelopmental diseases, including those manifested in adulthood.

52

53

54 Introduction

55 Cerebral development is a lifelong event beginning almost immediately after fertilization. During
56 the third embryonic week, neural tube is formed and before the end of the following week, it
57 compartmentalizes into forebrain, midbrain, and hindbrain. Beginning from the forebrain, the
58 telencephalon evolves towards a complex network with billions of neurons and glial cells in the
59 cerebral cortex, from which organized human thought and behavior will emerge. To a large
60 extent, the blueprint for the postnatal brain is laid out during gestation, when fetal neural cells
61 proliferate, differentiate, migrate, and make connections with other cells. These activities, for the
62 most part, appear to be genetically determined, epigenetically directed, and influenced by the
63 physical and chemical environment of the womb (Georgieff, 2007; Paridaen & Huttner, 2014).
64 Hence, the healthy development of central nervous system (CNS) in the period between the third
65 and seventh fetal week is likely to rely on adequate provisions of maternal resources like
66 vitamins or dietary elements.
67 Nutritional resources available to an embryo in these earliest weeks of life putatively determine
68 some of the most important aspects of future health. One well understood example that relates
69 maternal diet to CNS pathologies is spina bifida, caused by insufficient folic acid in early
70 pregnancy. While less understood, abnormalities in the levels of central minerals potentially
71 begin *in utero* (Radlowski & Johnson, 2013; Golub & Hogrefe, 2015). Examples of neurological
72 disorders where imbalances of micronutrients have been identified in adulthood include
73 Alzheimer's, Parkinson's and Huntington's diseases (Miller et al., 2006; Popescu et al., 2009;

Rosas et al., 2012). It is, however, difficult to assess target levels of trace elements in the developing human brain. Determining healthy levels of minerals and where and how they might be used in early development, while of clear importance, remains only superficially understood.

To date, the understanding of mineral inclusion as part of human brain development has only been carried out in post-mortem tissue, often involving brains treated with fixative, and inferred from animal models (Wróblewski, Chamberlain & Edström, 1984; Rajan et al., 1997). While great scientific advances on this subject have emerged from a variety of species, a number of peculiarities including cell types and a temporal organization that are uniquely human have been identified, becoming fundamental an in-depth study of these phenomena in human tissue. One method recently refined to model cellular and molecular events of human embryonic brain development is growing cerebral organoids *in vitro* (Eiraku et al., 2008; Lancaster et al., 2013). These three dimensional structures, derived from human pluripotent stem cells, progressively differentiate and self-organize into physiologically relevant cellular niches that mirror the developing human brain.

In the present work, we used Synchrotron Radiation based micro X-Ray Fluorescence (SR-XRF) analysis to detect and quantify trace elements present in human cerebral organoids. We sought to capture the levels and the distribution of minerals in brain tissue during a period of intense cell proliferation versus one in which early neuronal network formation was a dominant developmental feature. This work is the first description of mineral inclusion and distribution in human cerebral organoids.

96

97

98

Materials & Methods

Generation of human induced pluripotent stem cells

Human induced pluripotent stem cells (iPS) cells were obtained from a skin biopsy as described previously (Sochacki et al., 2016). Briefly, fibroblasts were maintained in culture and then transduced with CytoTune-iPS Sendai reprograming kit 2.0 (Thermo-Fischer) as per manufactor's instructions. Then, following colony formation and expansion, cells were checked for pluripotency markers via RT-PCR and ability to differentiate into embryoid bodies (S1 Fig). Skin tissue was obtained after donor signed an informed consent approved by the Research Ethics Committee of Hospital das Clínicas de Porto Alegre (CAPPesq, HCPA, IRB00000921) and by the Research Ethics Committee of Hospital Copa D'Or Rio de Janeiro (CEPCOPADOR, number 727.269).

110

Human pluripotent stem cells

Human embryonic stem cells (BR1 cell line) (Fraga et al., 2011) or iPS cells were cultured in mTSeR1 media (Stemcell Technologies) on Matrigel-coated surface (BD Biosciences). The

114 colonies were manually passaged every seven days and maintained at 37°C in humidified air
115 with 5% CO_2.

116

117 Human cerebral organoids

118 The differentiation into cerebral organoids was based in a previously described protocol
119 (Lancaster et al., 2013). However, differently from the latter study, most of the protocol was
120 conducted using spinner flasks under continuous rotation (Fig 1A). Briefly, human pluripotent
121 stem cells were dissociated with Accutase (Millipore) until obtaining single cells. Then,
122 approximately 250,000 cells/mL were inoculated into a spinner flask containing a final volume
123 of 50 mL of mTeSR1 supplemented with 10 μM Y-27632 (Rho-associated protein kinases
124 inhibitor, iRock) (Merck, Millipore) under uninterrupted rotation (40 rpm). After 24h, medium
125 was changed to Dulbecco's modified eagle medium (DMEM)/F12, supplemented with 20%
126 KnockOut™ Serum Replacement (KOSR, Invitrogen), 2 mM Glutamax (Invitrogen), 1%
127 minimum essential media nonessential amino acids (MEM-NEAA, Gibco), 55 μM 2-
128 Mercaptoethanol (Gibco) and 100 U/mL Penicillin-Streptomycin (Gibco). By day 6, embryoid
129 bodies (EB) were fed with DMEM/F12, 1x N2 supplement (Gibco), 2 mM Glutamax
130 (Invitrogen), 1% MEM-NEAA and 1 μg/mL heparin (Sigma) for 5 days. On day 11, cellular
131 aggregates were transferred to petri dishes and embedded in Matrigel for 1h at 37°C and 5%
132 CO_2. Then, cellular aggregates were decanted in a conical tube and returned to a spinner flask
133 containing differentiation media composed of 1:1 DMEM/F12: Neurobasal (Gibco), 0.5x N2, 1x
134 B27 minus vitamin A (Gibco), 2 mM Glutamax, 0.5% MEM-NEAA, 0.2 μM 2-Mercaptoethanol
135 and 2.5 μg/mL insulin. After 4 days, cell aggregates were grown in the aforementioned medium
136 except by replacing with B27 containing vitamin A (neurodifferentiation media) (Gibco). The

137 medium was changed every week. Cerebral organoids were grown until 30 days of
138 differentiation (totalizing 15 days in neurodifferentiation media) and 45 days (totalizing 30 days
139 in neurodifferentiation media) for analyses. The cerebral organoids derived from embryonic stem
140 cells were obtained from two independent assays.
141

142 Measurements of size and ventricular area of cerebral organoids

143 Cerebral organoids were transferred to non-adherent petri dishes and photographed with an
144 inverted microscopy (Eclipse TS100, Nikon). Using ImageJ software (NIH) the areas of cerebral
145 organoids were delimited with the freehand tool and the major diameter of cerebral organoids
146 was measured using the straight-line tool, with reference to the scale bar. The analyzed number
147 of cerebral organoids derived from human embryonic stem cells was as follows: 7-days old
148 organoids, n=107; 15-days old organoids, n=90; 30-days old organoids, n=56; 45-days old
149 organoids, n=18, obtained from two independent experiments. For cerebral organoids derived
150 from induced pluripotent stem cells, the number of cerebral organoids analyzed was as follows:
151 7-days old organoids, n=8; 15-days old organoids, n=15; 30-days old organoids, n=7; 45-days
152 old organoids, n=10, obtained from one experiment.
153 To measure the ventricular area of cerebral organoids, tissue sections were stained with
154 hematoxylin and eosin (H&E). Ventricles were considered as cavities surrounded by a layer of
155 radially organized cells. The area of ventricles was measured with ImageJ software through
156 delimitation with the freehand selection tool and was expressed as a proportion of total area of
157 the organoid measured in the same tissue slice (ventricles of 30-days old organoids: n=11;
158 ventricles of 45-days old organoids: n=31).
159

Immunohistochemistry

Cerebral organoids were fixed in 4% paraformaldehyde, incubated with sucrose solutions (10, 20 and 30%) in phosphate buffered saline (PBS), embedded in optimal cutting temperature compound (OCT) and frozen in liquid nitrogen. The organoids were sectioned with a cryostat (Leica) into 20 μm thick sections. Immunofluorescence was performed using the primary antibodies: anti-Nestin (MAB5326, Chemicon), anti-Pax6 (sc11357, Santa Cruz), anti-Tbr2 (AB2283, Millipore), anti-βIII-tubulin (T3952, Sigma Aldrich), anti-MAP2 (M1406, Sigma-Aldrich), anti-GAD67 (MAB5406, Chemicon), anti-glutamate (AB133, Chemicon), anti-synaptophysin (MAB368, Chemicon), anti-PSD95 (04-1066, Millipore) and anti-PH3 (06-570, Upstate). Secondary antibodies were used as follows: Alexa Fluor 488 Goat anti-mouse (A11001, Invitrogen) and Alexa Fluor 546 Goat anti-rabbit (A11010, Invitrogen). DAPI (4',6-diamidino-2-phenylindole, 1 mg/mL) was used for nuclei staining. Images were acquired using a high content automated microscope (Operetta - Perkin Elmer).

Positive cells for GAD67 and phosphorylated histone 3 (PH3) staining were quantified in the entire section of cerebral organoids. To quantify glutamate intensity, mean gray value (fluorescence intensity) was measured in three points of each cerebral organoid border, delimitated by a rectangular selection. The fluorescence intensity in the cerebral organoids' border was normalized for the tissue background and was given as fold increase on basal condition. The numbers of 30 and 45-days samples for quantifications were as follows: PH3 positive cells, n=3 and n=5; MAP2 area, n=4 and n=6; GAD67 positive cells, n=2 and n=4; glutamate fluorescence intensity, n=6 and n=7, respectively.

Synchrotron Radiation X-ray Fluorescence Spectroscopy (SR-XRF) analysis

For XRF analysis, cerebral organoids were quickly washed in PBS, embedded in OCT and frozen. Tissue sections of 30 μm thick were placed into ultralene film (transparent to X-ray) and air-dried.

The SR-XRF analyses were performed at the D09B X-Ray fluorescence beamline of the Brazilian Synchrotron Light Source (Pérez et al., 1999) (Campinas, Brazil) using standard temperature and pressure conditions. Samples were excited by a white beam with energy ranging from 5 keV to 17 keV and an optical system based on a pair of bent mirrors in a Kirkpatrick-Baez arrangement to focus the X-ray beam down to 20 μm spatial resolution. Each spot was irradiated by one second. A silicon drift detector (KETEK GmbH) with 140 eV (FWHM) at 5.9 keV placed at 90^{o} from the incident beam was used to collect X-ray fluorescent and scattered radiation coming from samples. Information of elemental concentrations was collected from each pixel to generate corresponding XRF maps. The maps were constructed by plotting the fluorescence intensity at each point of the scan. All the spectra were analyzed using the PyMca program developed by the Software Group of the European Synchrotron Radiation Facility.

Image analyses of trace elements distribution

Images of colored heat maps were converted to grayscale images with Adobe Photoshop CS5 by manually adjusting the hue to match the colors' intensity in RGB images. Then, ImageJ software was used to obtain the intensity profiles by drawing a line in sagittal and coronal planes of the organoids images. The generated plot profiles were analyzed in Igor Pro 6 software

(Wavemetrics, Lake Oswego, OR, USA) to create curve fittings with polynomial regression of 3 terms. The resulting curves were classified as concave or convex. If the fitting result gave rise to a line with less than 10 points of inclination, it was considered as a straight line. We assumed concave as peripheral, convex as central and straight as diffused distribution of the elements inside the cerebral organoids sections.

Inter-elemental analysis

In order to carry out quantifiable comparisons between elements' levels inferred from synchrotron derived heat maps, images were converted from pseudo gray scale in PNG to grayscale in TIFF format. Grayscale values were re-normalized according to the calibration bar within the images. All images were visually inspected for congruence in spatial organization and signal intensities when compared with colored heat maps. In TIFF format, images were imported to Igor Pro 6 software (Wavemetrics, Lake Oswego) which transformed the data set into a series of waves containing ordered (0-255) grayscale values. Waves in this context represented a single column from the image. To compare between images, all waves from an image were concatenated and stored as a single vector. In this form, images were exported from Igor Pro 6 into either Matlab or R where normality of grayscale values corresponding to each image (Shapiro Wilks, R) along with correlations were carried out using existing functions within the respective softwares.

Statistical Analyses

Results depicted in Table 2 and 3 were expressed as mean ± S.D. Graphic representations of quantifications correspond to mean ± S.D. Analyses of statistical significance were obtained using GraphPad Prism 4 software (GraphPad Software, La Jolla California, USA). Comparisons among organoids' sizes at 7, 15, 30 and 45 days of differentiation were analyzed using one-way ANOVA followed by Tukey's post hoc test.

Results

The growth of human cerebral organoids

Exogenous organogenesis using pluripotent stem cells has emerged as a breakthrough technology to study aspects of human brain development in a dynamic and living state

(Lancaster et al., 2013). In our preparations, cerebral organoids' differentiation from human embryonic stem cells occurred in spinner flasks as represented in Fig 1A, and by the end of 45 days presented spheroid morphology (Fig 1B). In detail, 30-days old organoids demonstrated different hues and internal folding, suggestive of different cell layers (Figs 1C and C'). Periods of accelerated growth were observed between the 7th and the 15th day, followed by a period of stationary growth upon retinoic acid addition (15 to 30 days). Then, organoids continued to expand in size from day 30 to day 45, reaching (1,240 ± 365) μm in diameter (Fig 1D). Cerebral organoids derived from iPS cells also grew in a similar fashion (S2 Fig).

As one of our major goals was to generate a cortical anlage from human embryonic stem cells *in vitro*, we then examined the cytoarchitecture of the generated cerebral organoids. We focused on two separate time points, 30 and 45 days of differentiation, which corresponded to 15 and 30 days, respectively, of exposure to retinoic acid, a crucial morphogen to neuronal induction. After 30 days, prominent circular structures reminiscent of early ventricle formation were observed (Fig 2A). Following organoids' maturation, larger ventricles were replaced by narrow ones of reduced sizes (Figs 2B-C). The intermediate filament nestin, characteristic of CNS progenitors, was expressed all over the developing organoids (Fig 3A). Similar to the cortical development *in vivo*, areas immediately adjacent to the putative ventricles had greater cell density and exhibited a radial and outward polarization suggestive of zones of cellular division and migration. Indeed, the presence of apical progenitors was characterized by mitotic cells lining the luminal surface, positively stained for PH3 (Fig 3B), and by the expression of the transcription factor PAX6 in the ventricular zone (Fig 3C). Furthermore, intermediate progenitors expressing the T-box homeobox protein TBR2 were found on the way to the subventricular zone, positioned radially to the luminal surface and adjacent to tangentially migrating neurons (MAP2 positive cells) (Fig

3D) in a cellular architecture similar to the cortical plate *in vivo* (Lui, Hansen & Kriegstein, 2011). Likewise, in organoids derived from iPS cells, differentiated neurons were positioned in the outer rim of the cellular layer around the putative ventricle, whereas neural progenitors occupied the innermost portion (S2 Fig).

In 45-days old organoids, MAP2 staining identified the neuronal primordial plexiform layer on the surface (Fig 4A), while migratory GABAergic neurons were detected by glutamic acid decarboxylase 67 (GAD67) staining in different places inside the organoids, primarily near the ventricles (Fig 4B). Concurrently, glutamate was detected in the outermost perimeter of the organoid (Fig 4C). Synaptogenesis was observed by the presence of synaptophysin, a component of presynaptic vesicles, and also by the detection of the postsynaptic density protein 95 (PSD95) (Fig 4D).

As a result of the progress from a self-renewal stage of neural progenitors toward neuronal differentiation, a decrease of 5 times in mitotic activity was observed when comparing the organoids at 30 and 45 days of differentiation (Fig 5A). Accordingly, the amount of mature neurons tripled, as indicated by MAP2 staining (Fig 5B) and the number of neurons expressing GAD67 increased four times (Fig 5C), when comparing organoids at the 30^{th} and at 45^{th} day of differentiation. In addition, the peripheral glutamate staining increased 2.5 times (Fig 5D). In line with these data, we considered these two time points (30 and 45 days) to depict two distinct developmental phases, one of pronounced cell division dedicated to tissue expansion versus other of early neuronal network formation in cerebral organogenesis. Then, we asked whether these two time points might show different elemental distribution as they represent two demarcated developmental stages.

SR-XRF microprobe analysis

290 SR-XRF microprobe was used to scan elemental composition in cerebral organoids as
291 characteristic X-rays profiles provide a unique identifying signature for a species of atom. XRF
292 analysis revealed that the major trace elements in cerebral organoids were Phosphorus (P), Sulfur
293 (S), Potassium (K), Iron (Fe), Calcium (Ca) and Zinc (Zn). The elements Manganese (Mn),
294 Nickel (Ni) and Copper (Cu) were detectable in our preparations, but were not be considered
295 further in this study due to their extremely low levels and subsequent classification as ultratrace
296 elements. Although Chlorine (Cl) was also detected, it was disregarded for further analysis as it
297 is considered a potential laboratorial artifact. While the specific roles and importance of the
298 detected trace elements for brain development or function may be under characterization, some
299 of the known functions are summarized in Table 1.
300

301 Trace elements distribution in human cerebral organoids

302 To search for trends in patterns of concentration gradients across cerebral organoids, the spectral
303 profile corresponding to each measurable element was collected and assembled into heat maps of
304 the readable field, as represented in Fig 6. Phosphorus could be detected all over organoids'
305 extension, despite being concentrated within the external border in both 30 and 45-day time
306 points. Potassium levels were distributed diffusely as well; however, after 30 days it was higher
307 in the organoids' border and then became evenly distributed. Sulfur, Ca and Fe displayed a more
308 homogeneous distribution, with low levels throughout the cerebral organoids in both
309 proliferative and neuronal differentiation phases. Meanwhile, Zn was mostly diffused in 30-days
310 old organoids and became peripheral along differentiation process in 45-days old organoids.
311 Patterns of elements' distribution were useful to show a tendency for diffuseness for most, with

the exceptions of P and Zn. Rather than spreading internally, these two elements continued to be located in higher concentrations towards the outer edge of the cerebral organoids.

Elemental concentration in cerebral organoids

To compare the contribution of elements in, here named, proliferative (30 days) and neuronal maturation (45 days) stages, we estimated concentrations of trace elements in parts per million (ppm), which are shown in Table 2. Phosphorus, S and K were more abundant in both 30 days ((16,142±1,219) ppm; (4,955±350) ppm and (6,120±1,745) ppm, respectively) and 45 days ((10,286±840) ppm; (4,462±249) ppm and (3,951±422) ppm, respectively). Calcium, Fe and Zn were found in relatively low levels ((192±157) ppm, (84±61) ppm and (129±6) ppm in 30-days old organoids; (286±43) ppm, (87±37) ppm and (101±2) ppm in 45-days old organoids, respectively). In general, the levels of trace elements tend to diminish from 30 to 45 days of differentiation.

To determine to which degree the presence of trace elements in cerebral organoids could be due to passive diffusion from media or to active cellular metabolism, we compared elements' availability in culture medium with the amounts found within the organoids. According to manufacturers' information, the concentrations available in culture media were as follows: P: 129 ppm, S: 25 ppm, K: 356 ppm, Ca: 161 ppm, Fe: 0.28 ppm, and Zn: 0.31 ppm. When compared to the data exhibited in Table 2, the concentrations found in cerebral organoids presented a much higher magnitude.

Inter-elemental relationship

From an initial inspection of the spatial distribution of each element, it was not possible to assess, with any confidence, to which extent they may interact functionally or chemically, as would occur when they become part of biomolecules. We then used correlation analysis as a metric to quantify coincidence in spatial locations for pairs of elements. Pearson's correlation coefficients were positive in direction. In this assessment, we interpreted r-values greater than 0.5 as indicators of potentially meaningful associations in spatial grouping. We observed that correlation coefficients greater than 0.5 could be detected in the 30-days old organoids, however; stable associations across cerebral organoids were not always seen. Table 3 provides a summary of the data regarding correlations found for pairs of elements. Interestingly, coefficient values for all combinations of elements were higher in 45-days old organoids and standard deviations across organoids were also lower in the latter case.

Discussion

Implications of trace elements detected in cerebral organoids to cerebral organogenesis

While it is generally accepted that micronutrients are vital to brain morphogenesis, neurochemistry and neurophysiology, well-controlled studies in humans are still needed. Furthermore, since most studies on this subject have been done on adult-state or postmortem tissue samples, little is known about the elemental composition of the developing human CNS. Though it is not an exact replica of a human embryonic brain, exogenously developed cerebral organoids undergo many developmental stages and events that parallel the human condition. Perhaps more importantly, the circuits and structures being constructed contain a significant portion of the human genetic blueprinting and specific neurons that make up the early neuronal networks that give rise to the brain (Lancaster et al., 2013). Therefore, the model used in this study, amongst others of human organogenesis, could be argued to be the closest and most complete study system to date for understanding human neural development and its pathological manifestations.

The methodology for development of cerebral organoids' tissues described in here subtly deviates from the original method reported by Lancaster et al. (2013). Specifically, the aggregation of dissociated pluripotent stem cells into EBs was conducted in spinner flasks instead of using individualized non-adherent wells of 96-well plates. The EBs obtained here with

iPS cells presented similar sizes ((514 ± 76)μm in diameter, S2 Fig) when compared to Lancaster's descriptions for those derived from the H9 cell line (Lancaster & Knoblich, 2014). However, EBs obtained from the BR1 cell line were relatively smaller ((290 ± 80) μm diameter, Fig 1). One possibility is that these results may reflect inter-lineage variability in the aggregation potential of pluripotent stem cell lines, as described by others (Cahan & Daley, 2013). Regardless of this difference in the EB size, by the end of 30 and 45 days, the cytoarchitecture of cerebral organoids' was similar to the original report (Lancaster et al., 2013).

SR-XRF is a suitable technique to scan and image trace elements in brain tissue and has been applied in many models with neurological diseases. The primary advantages in using SR-XRF lie in its low limit of detection, topographic high-resolution chemical imaging and recognition of metal compounds irrespectively of oxidation state. Given that metal metabolism is disrupted in prevalent neurodegenerative disorders, such as Alzheimer's, Huntington's and Parkinson's diseases (Popescu et al., 2009; Wang et al., 2012; Muller & Leavitt, 2014), SR-XRF can also be applied for a comprehensive view of metal homeostasis in brain development and aging. Contrary to the research aims carried out by other groups, our study intended to employ SR-XRF on human cerebral organoids to provide us with the first glimpse into which elements may play active roles in early brain development. More specifically, we report here that phosphorus, potassium, calcium, iron, zinc and sulfur take part in neural composition during cerebral organoids' formation.

Phosphorus was the most heavily represented element. When comparing phosphorus levels detected on proliferative (30 days) and neuronal differentiation (45 days) stages, it was significantly decreased. Since phosphorus is a structural component of major biomolecules, such as nucleotides and phospholipids, this observed reduction might be explained by a switch from a

396 phase of intense synthesis, including DNA and phospholipidic production, to a more migratory
397 and differentiating phase. With respect to tissue growth, phosphorus levels in cerebral organoids
398 were in the same concentration range (mg/g) of that reported for adult brains (Rajan et al., 1997),
399 albeit having been noted here in a higher quantity (Table 2). In this regard, the levels found in
400 our study imply a greater participation of phosphorus during the development of neural tissue
401 (Rajan et al., 1997). Silvestre et al. also showed that total lipid phosphorus content is higher in
402 the embryonic brain than in adult brain cells (Silvestre, Maccioni & Caputto, 2009). As the
403 developing brain contains superior concentrations of phosphate groups belonging to lecithins,
404 cephalins and sphingomyelins, this could explain the different values found in our study. This
405 dissimilarity underscores the need for pursuing elemental changes at either end of the aging
406 spectrum.
407 Cerebral organoids were also shown to contain significant levels of potassium and sulfur.
408 Potassium is essential to transmembrane transport, regulation of cellular volume and membrane
409 resting potential. During brain ontogenesis, potassium regulates proliferation of neural
410 progenitors (Achilles et al., 2007; Yasuda, Bartlett & Adams, 2008; Schaarschmidt et al., 2009)
411 and is maintained in heightened levels in rapidly dividing cells (Cameron, Pool & Smith, 1979;
412 Wallberg et al., 2000). As potassium currents also support the migration of early neurons over
413 long distances due to cellular volume change (Hendriks, Morest & Kaczmarek, 1999), we can
414 speculate from our data that potassium could be important to maintain mitotic activity at 30-days
415 old organoids and to promote cell migration at 45-days old organoids, amongst other roles.
416 It is known that sulfur integrates virtually all proteins through methionine and cysteine amino
417 acids and disulfide bounds. In the embryonic cerebrum, chondroitin sulfate proteoglycans anchor
418 attractive and/or repulsive cues such as growth factors, chemokines, axon guidance molecules,

and cell adhesion molecules important for neuronal migration in strategically routes such as the striatum, marginal zone, subplate and subventricular zone in the neocortex (Maeda, 2015). As an example, brains devoid of perlecan, a heparin sulfate proteoglycan component of the CNS extracellular matrix, have impaired cortical development and are microcephalic (Girós et al., 2007). Beyond this, sulfur is also incorporated in proteoglycans expressed in the basal lamina of the neuroepithelium that regulate neurogenesis in the developing telencephalon (Girós et al., 2007). In cerebral organoids, we found high levels of sulfur, both in 30 and 45 days of differentiation, pointing to its central role in organoids' patterning. However, there was a modest reduction of sulfur levels in cerebral organoids between 30 and 45 days, which may suggest that sulfur is more necessary when cell division is prominent (Table 2). Therefore, we postulate that sulfur may play a fundamental role in brain construction and in organoids' scaffolding and patterning.

The metallic elements calcium, iron and zinc, which are essential for brain morphogenesis, were found in the μg/g range in cerebral organoids. Calcium participates in a variety of cellular functions in different areas extending from proliferative zones to post mitotic intermediate zone and marginal zone. In neural progenitor cells, calcium waves, sustained by IP3-signaling, control cell proliferation (Weissman et al., 2004; Resende et al., 2010), while calcium influx via ion channels influences cell differentiation (Shin et al., 2010). Importantly, during early neurogenesis, the expression of transcription factors regulating neuronal survival and differentiation can be controlled by calcium (Leclerc et al., 2012). Noteworthy, the ppm values of calcium detected here are consistent with those found by Riederer et al. (1989) and Rajan et al. (1997) (Riederer et al., 1989; Rajan et al., 1997) (Table 2). Altogether, these findings and our data emphasizes that calcium may pave the way to brain organogenesis.

Also of interest, zinc and iron, essential metals to brain morphogenesis, were detected in cerebral organoids. Zinc is an essential element to protein synthesis, enzymatic catalysis and a structural factor to zinc finger transcriptional factors. Zinc dependent enzymes include metalloproteinases and many dehydrogenases of intermediary metabolism (Tapiero & Tew, 2003) important for CNS function. In addition, it is released in the synaptic cleft and modulates many synaptic activities (Marger, Schubert & Bertrand, 2014). In comparison to previous studies in adult brain, we found higher levels of zinc in cerebral organoids, although compatible in scale of dosage (Table 2). While higher concentrations of zinc in adult brain are toxic to neural cells and also cause axonal degeneration in mice (Chuah, Tennent & Jacobs, 1995), zinc modulates stem cell proliferation and neuronal differentiation during neurogenesis (Gao et al., 2009; Levenson & Morris, 2011; Morris & Levenson, 2013). In accordance, previous data from our group have demonstrated increased zinc during neural differentiation of human pluripotent stem cells (Cardoso et al., 2011). This may highlight the importance of zinc for neural stem cells commitment and justify why the levels found in cerebral organoids are subtly higher than those described in adult brain (Table 2) (Dexter et al., 1991; Rajan et al., 1997; Rahil-Khazen et al., 2002).

It is currently known that iron accumulates during prenatal development of the brain, with the highest levels observed immediately after birth. In the developing brain, iron is required in rapidly developing regions such as the cerebral cortex (Siddappa et al., 2003) in heme-containing cytochromes that regulate neuronal and glial energetic status (Evans & Mackler, 1985). Along the same line, iron is required to the initial expansion of neural tissue and by neurogenesis, which may account for its levels in the present study. It is noteworthy that the iron values found for cerebral organoids parallel those measured in the adult brain (Sofic et al., 1988; Dexter et al.,

1991; Rajan et al., 1997; Rahil-Khazen et al., 2002). It is worth mentioning that higher iron concentrations are found in some specific cerebral regions such as Substantia nigra, Putamen and Globus pallidus (Dexter et al., 1991), not represented in this study. Iron-containing enzymes are essential for tyrosine and tryptophan hydroxylases activities and for monoamine catabolism in synapses. However, iron is also required for ribonucleotide reductase to regulate cell division and for normal myelination throughout CNS development (Lozoff & Georgieff, 2006).

Trace elements distribution in human cerebral organoids

Our data indicate that trace elements change their distribution inside organoids along differentiation. It is known that some molecules can pass through cell membrane by simple diffusion or with the aid of specific cellular transporters or channels. Potassium was firstly concentrated at the organoids' border and then became evenly distributed inside. Since potassium is positively charged and therefore not permeant to cell membranes, one possibility is that NKCC1, an inwardly directed cotransporter, begins to be expressed and might contribute to the simultaneous potassium and chloride influx. NKCC1 expression is upregulated in early developmental stages and downregulated in later brain development in vivo (Kaila et al., 2014).
Besides the distribution profile of an atomic element being associated with changes in the expression of receptors and specific channels, one can also suggest a role of such element in a particular cellular niche. For example, zinc displayed a more homogeneous distribution inside organoids, but became relatively higher in organoids' periphery on 45 days. Of note, glutamate was almost undetectable in organoids at 30 days of differentiation, but at 45 days, it occupied the outer portion of the organoids. It is known that zinc is present at high levels in glutamatergic synaptic vesicles of forebrain neurons and that its influx can be mediated by AMPA channels

(Martínez-Galán, Díaz & Juiz, 2003; Takeda et al., 2009). Beyond this, zinc-dependent metalloproteinases facilitate neural migration and regulate neurite outgrowth (Sanz, Ferraro & Fournier, 2015; Sîrbulescu, Ilieş & Zupanc, 2015) in the pre-plate and cortical plate. Hence, one possibility is that zinc intensity matches cellular distribution of glutamatergic cells and neuronal synaptogenesis. In this regard, further studies should help identify differential changes in the expression of specific channels and receptors that may take part in microelemental homeostasis of cerebral organoids.

Inter-elemental correlations in human cerebral organoids

The atomic elements can exist freely intra and extracellular in the form of ions or ionic groups and in association with proteins, for example. In 30-days old organoids, there was a high spatial correlation between the elements phosphorus and zinc ($r > 0.8$, Table 3). Zinc is not only a structural element, but also acts as a regulator of cell proliferation. Based on studies with zinc chelators in mammalian cells, it was found that zinc deficiency results in reduced expression of thymidine kinase (Chesters, Petrie & Travis, 1990) and reduction in thymidine incorporation (Chesters, Petrie & Vint, 1989). Strictly, zinc integrates DNA polymerase (Springgate et al., 1973), RNA polymerase (Wu et al., 1992), and ribosomal proteins (Härd et al., 2000). Whilst purely speculative, it is possible that phosphorus, as being part of nucleic acids and present in proteins, share the same location with zinc, as both are involved in cell proliferation and protein synthesis. Another interesting example is potassium, which seems to be directly involved in the control of protein synthesis (Lubin & Ennis, 1964) and, in conjunction with phosphorus, are enriched in ribosomes. Specifically in neurons, potassium tends to correlate with phosphorus in the adult rat brain (Cameron, Sheridan & Smith, 1978) as we observed in the cerebral organoids.

511

512 Functional significance

513 Mounting evidence indicates that maternal malnutrition may be causative in many
514 neurocognitive deficits and neurological diseases in offspring (Felt & Lozoff, 1996; de Souza,
515 Fernandes & do Carmo, 2011). Given that maternal diet is the principle source of dietary
516 elements available to a developing fetus, our data highlight the importance of matching the
517 essential elements phosphorus, potassium, calcium, iron, zinc and sulfur to developmental needs
518 of the brain. For instance, deficiencies in zinc nutrition during prenatal development are
519 associated with offspring learning and memory paucity (Liu et al., 1992; Tahmasebi Boroujeni et
520 al., 2009; Yu et al., 2013), in part caused by decreased expression of brain-derived neurotrophic
521 factor (BDNF), altered myelin composition (Liu et al., 1992) and declined long-term potentiation
522 (Yu, Ren & Yu, 2013). Gestational iron anemia, the most common nutritional need, can impact
523 learning, memory and motor abilities in progeny. These poor executive performances can be
524 explained at the cellular level by decreased synaptic maturity, dopamine metabolism and myelin
525 composition (Lozoff & Georgieff, 2006). In a prospectively study, it was found that maternal
526 iron deficiency may be a risk for schizophrenia in offspring (Insel et al., 2008). This means that
527 mother's diet during pregnancy can have long-term consequences in fetal brain structuring.

528

529 Conclusions

530 Here, we have shown the potential of cerebral organoids in conjunction to XRF analysis to
531 explore minerals homeostasis during brain development. Mapping the location of each
532 micronutrient could be useful for determining receptor and specific channels expressions, as well

as for locating elements that take part in neural composition during cerebral organogenesis, such as phosphorus, potassium, calcium, iron, zinc and sulfur in a particular cellular niche. Besides, mathematical analyses such as spatial correlations for pairs of elements could give a glimpse of chemical or functional interactions.

The levels of trace elements in normal and pathological brain development are central to establishing cause and effect relationships, mainly for nutritional deficiencies or metal transporters inabilities and disorders in which trace elements are involved. Nowadays, many diseases have been regarded as neurodevelopmental disorders, with its roots planted in the first months or years of life. Disturbances in early brain development have been deemed important for later developing Parkinson's disease or schizophrenia (Piper et al., 2012; Le Grand et al., 2015). Therefore, it seems reasonable to emphasize the need to gather data on normal trace elemental levels in embryonic brain tissue as the data presented here. In conclusion, cerebral organoids derived from pluripotent stem cells recapitulate features of trace elements' distribution previously described in the human brain.

Acknowledgments

We are indebted to Ismael Gomes, Gabriela Lopes Vitória, Marcelo Costa and Jarek Sochacki for taking excellent care of cell lines.

554

References

Achilles K, Okabe A, Ikeda M, Shimizu-Okabe C, Yamada J, Fukuda A, Luhmann HJ, Kilb W. 2007. Kinetic properties of Cl uptake mediated by Na+-dependent K+-2Cl cotransport in immature rat neocortical neurons. *The Journal of neuroscience : the official journal of the Society for Neuroscience* 27:8616–8627. DOI: 10.1523/JNEUROSCI.5041-06.2007.

Atlas D. 2013. The voltage-gated calcium channel functions as the molecular switch of synaptic transmission. *Annual review of biochemistry* 82:607–35. DOI: 10.1146/annurev-biochem-080411-121438.

Cahan P, Daley GQ. 2013. Origins and implications of pluripotent stem cell variability and heterogeneity. *Nature reviews. Molecular cell biology* 14:357–68. DOI: 10.1038/nrm3584.

Cameron IL, Pool TB, Smith NK. 1979. An X-ray microanalysis survey of the concentration of elements in the cytoplasm of different mammalian cell types. *Journal of cellular physiology* 101:493–501. DOI: 10.1002/jcp.1041010315.

Cameron IL, Sheridan PJ, Smith NR. 1978. An x-ray microanalysis study of differences in concentration of elements in brain cells due to opiates, cell type, and subcellular location. *Journal of neuroscience research* 3:397–410.

Cardoso SC, Stelling MP, Paulsen BS, Rehen SK. 2011. Synchrotron radiation X-ray microfluorescence reveals polarized distribution of atomic elements during differentiation of pluripotent stem cells. *PLoS ONE* 6:1–10. DOI: 10.1371/journal.pone.0029244.

Chesters JK, Petrie L, Travis AJ. 1990. A requirement for Zn2+ for the induction of thymidine kinase but not ornithine decarboxylase in 3T3 cells stimulated from quiescence. *The Biochemical journal* 272:525–7.

Chesters JK, Petrie L, Vint H. 1989. Specificity and timing of the Zn2+ requirement for DNA synthesis by 3T3 cells. *Experimental cell research* 184:499–508.

Chuah MI, Tennent R, Jacobs I. 1995. Response of olfactory Schwann cells to intranasal zinc sulfate irrigation. *Journal of neuroscience research* 42:470–8. DOI: 10.1002/jnr.490420405.

Dexter DT, Carayon A, Javoy-Agid F, Agid Y, Wells FR, Daniel SE, Lees AJ, Jenner P, Marsden CD. 1991. Alterations in the levels of iron, ferritin and other trace metals in Parkinson's disease and other neurodegenerative diseases affecting the basal ganglia. *Brain : a journal of neurology* 114 (Pt 4:1953–75.

Eiraku M, Watanabe K, Matsuo-Takasaki M, Kawada M, Yonemura S, Matsumura M, Wataya T, Nishiyama A, Muguruma K, Sasai Y. 2008. Self-organized formation of polarized

589 cortical tissues from ESCs and its active manipulation by extrinsic signals. *Cell stem cell*
590 3:519–32. DOI: 10.1016/j.stem.2008.09.002.

591 Erikson KM, Jones BC, Hess EJ, Zhang Q, Beard JL. 2001. Iron deficiency decreases dopamine
592 D1 and D2 receptors in rat brain. *Pharmacology, biochemistry, and behavior* 69:409–18.

593 Evans TC, Mackler B. 1985. Effect of iron deficiency on energy conservation in rat liver and
594 skeletal muscle submitochondrial particles. *Biochemical medicine* 34:93–9.

595 Felt BT, Lozoff B. 1996. Brain iron and behavior of rats are not normalized by treatment of iron
596 deficiency anemia during early development. *The Journal of nutrition* 126:693–701.

597 Fraga AM, Sukoyan M, Rajan P, Braga DP de AF, Iaconelli A, Franco JG, Borges E, Pereira L
598 V. 2011. Establishment of a Brazilian line of human embryonic stem cells in defined
599 medium: implications for cell therapy in an ethnically diverse population. *Cell*
600 *transplantation* 20:431–40. DOI: 10.3727/096368910X522261.

601 Gao H-L, Zheng W, Xin N, Chi Z-H, Wang Z-Y, Chen J, Wang Z-Y. 2009. Zinc deficiency
602 reduces neurogenesis accompanied by neuronal apoptosis through caspase-dependent and -
603 independent signaling pathways. *Neurotoxicity research* 16:416–25. DOI: 10.1007/s12640-
604 009-9072-7.

605 Georgieff MK. 2007. Nutrition and the developing brain: nutrient priorities and measurement.
606 *The American journal of clinical nutrition* 85:614S–620S.

607 Girós A, Morante J, Gil-Sanz C, Fairén A, Costell M. 2007. Perlecan controls neurogenesis in
608 the developing telencephalon. *BMC developmental biology* 7:29. DOI: 10.1186/1471-213X-
609 7-29.

610 Golub MS, Hogrefe CE. 2015. Fetal iron deficiency and genotype influence emotionality in
611 infant rhesus monkeys. *The Journal of nutrition* 145:647–53. DOI: 10.3945/jn.114.201798.

612 Le Grand JN, Gonzalez-Cano L, Pavlou MA, Schwamborn JC. 2015. Neural stem cells in
613 Parkinson's disease: a role for neurogenesis defects in onset and progression. *Cellular and*
614 *molecular life sciences : CMLS* 72:773–97. DOI: 10.1007/s00018-014-1774-1.

615 Härd T, Rak A, Allard P, Kloo L, Garber M. 2000. The solution structure of ribosomal protein
616 L36 from Thermus thermophilus reveals a zinc-ribbon-like fold. *Journal of molecular*
617 *biology* 296:169–80. DOI: 10.1006/jmbi.1999.3433.

618 Hendriks R, Morest DK, Kaczmarek LK. 1999. Role in neuronal cell migration for high-
619 threshold potassium currents in the chicken hindbrain. *Journal of neuroscience research*
620 58:805–14.

621 Inatani M, Irie F, Plump AS, Tessier-Lavigne M, Yamaguchi Y. 2003. Mammalian brain
622 morphogenesis and midline axon guidance require heparan sulfate. *Science (New York,*
623 *N.Y.)* 302:1044–1046. DOI: 10.1126/science.1090497.

624 Insel BJ, Schaefer C a, McKeague IW, Susser ES, Brown AS. 2008. Maternal iron deficiency
625 and the risk of schizophrenia in offspring. *Archives of general psychiatry* 65:1136–1144.
626 DOI: 10.1001/archpsyc.65.10.1136.

627 Kaila K, Price TJ, Payne J a, Puskarjov M, Voipio J. 2014. Cation-chloride cotransporters in
628 neuronal development, plasticity and disease. *Nature Publishing Group* 15:637–654. DOI:
629 10.1038/nrn3819.

630 Lancaster MA, Renner M, Martin C-A, Wenzel D, Bicknell LS, Hurles ME, Homfray T,
631 Penninger JM, Jackson AP, Knoblich JA. 2013. Cerebral organoids model human brain
632 development and microcephaly. *Nature* 501:373–9. DOI: 10.1038/nature12517.

633 Lancaster MA, Knoblich JA. 2014. Generation of cerebral organoids from human pluripotent
634 stem cells. *Nature protocols* 9:2329–2340. DOI: 10.1038/nprot.2014.158.

635 Leclerc C, Néant I, Moreau M, Hansen D V, Lui JH, Parker PRL, Kriegstein AR. 2012. The
636 calcium: an early signal that initiates the formation of the nervous system during
637 embryogenesis. *Frontiers in Molecular Neuroscience* 5:1–12. DOI:
638 10.3389/fnmol.2012.00064.

639 Levenson CW, Morris D. 2011. Zinc and Neurogenesis: Making New Neurons from
640 Development to Adulthood. *Advances in Nutrition: An International Review Journal* 2:96–
641 100. DOI: 10.3945/an.110.000174.

642 Liu H, Oteiza PI, Gershwin ME, Golub MS, Keen CL. 1992. Effects of maternal marginal zinc
643 deficiency on myelin protein profiles in the suckling rat and infant rhesus monkey.
644 *Biological trace element research* 34:55–66. DOI: 10.1007/BF02783898.

645 Lozoff B, Georgieff MK. 2006. Iron Deficiency and Brain Development. *Seminars in Pediatric*
646 *Neurology* 13:158–165. DOI: 10.1016/j.spen.2006.08.004.

647 Lubin M, Ennis HL. 1964. on the Role of Intracellular Potassium in Protein Synthesis.
648 *Biochimica et biophysica acta* 80:614–631. DOI: 10.1016/0926-6550(64)90306-8.

649 Lui JH, Hansen D V., Kriegstein AR. 2011. Development and evolution of the human neocortex.
650 *Cell* 146:18–36. DOI: 10.1016/j.cell.2011.06.030.

651 Maeda N. 2015. Proteoglycans and neuronal migration in the cerebral cortex during development
652 and disease. *Frontiers in Neuroscience* 9:1–15. DOI: 10.3389/fnins.2015.00098.

653 Marger L, Schubert CR, Bertrand D. 2014. Zinc: an underappreciated modulatory factor of brain
654 function. *Biochemical pharmacology* 91:426–35. DOI: 10.1016/j.bcp.2014.08.002.

655 Martínez-Galán JR, Díaz C, Juiz JM. 2003. Histochemical localization of neurons with zinc-
656 permeable AMPA/kainate channels in rat brain slices. *Brain research* 963:156–64.

657 Miller LM, Wang Q, Telivala TP, Smith RJ, Lanzirotti A, Miklossy J. 2006. Synchrotron-based
658 infrared and X-ray imaging shows focalized accumulation of Cu and Zn co-localized with
659 β-amyloid deposits in Alzheimer's disease. *Journal of Structural Biology* 155:30–37. DOI:
660 10.1016/j.jsb.2005.09.004.

661 Morris DR, Levenson CW. 2013. Zinc regulation of transcriptional activity during retinoic acid-
662 induced neuronal differentiation. *Journal of Nutritional Biochemistry* 24:1940–1944. DOI:
663 10.1016/j.jnutbio.2013.06.002.

664 Muller M, Leavitt BR. 2014. Iron dysregulation in Huntington's disease. *Journal of*
665 *neurochemistry* 130:328–50. DOI: 10.1111/jnc.12739.

666 Paridaen JTML, Huttner WB. 2014. Neurogenesis during development of the vertebrate central
667 nervous system. *EMBO reports* 15:351–64. DOI: 10.1002/embr.201438447.

668 Pérez CA, Radtke M, Sánchez HJ, Tolentino H, Neuenshwander RT, Barg W, Rubio M, Bueno
669 MIS, Raimundo IM, Rohwedder JJR. 1999. Synchrotron radiation X-Ray fluorescence at
670 the LNLS: beamline instrumentation and experiments. *X-Ray Spectrometry* 28:320–326.
671 DOI: 10.1002/(SICI)1097-4539(199909/10)28:5<320::AID-XRS359>3.0.CO;2-1.

672 Piper M, Beneyto M, Burne THJ, Eyles DW, Lewis D a., McGrath JJ. 2012. The
673 Neurodevelopmental Hypothesis of Schizophrenia. Convergent Clues from Epidemiology
674 and Neuropathology. *Psychiatric Clinics of North America* 35:571–584. DOI:
675 10.1016/j.psc.2012.06.002.

676 Popescu BFG, George MJ, Bergmann U, Garachtchenko A V, Kelly ME, McCrea RPE, Lüning
677 K, Devon RM, George GN, Hanson AD, Harder SM, Chapman LD, Pickering IJ, Nichol H.
678 2009. Mapping metals in Parkinson's and normal brain using rapid-scanning x-ray
679 fluorescence. *Physics in medicine and biology* 54:651–663. DOI: 10.1088/0031-
680 9155/54/3/012.

681 Radlowski EC, Johnson RW. 2013. Perinatal iron deficiency and neurocognitive development.
682 *Frontiers in human neuroscience* 7:585. DOI: 10.3389/fnhum.2013.00585.

683 Rahil-Khazen R, Bolann BJ, Myking A, Ulvik RJ. 2002. Multi-element analysis of trace element
684 levels in human autopsy tissues by using inductively coupled atomic emission spectrometry
685 technique (ICP-AES). *Journal of trace elements in medicine and biology : organ of the*
686 *Society for Minerals and Trace Elements (GMS)* 16:15–25. DOI: 10.1016/S0946-
687 672X(02)80004-9.

688 Rajan MT, Jagannatha Rao KS, Mamatha BM, Rao R V, Shanmugavelu P, Menon RB, Pavithran
689 M V. 1997. Quantification of trace elements in normal human brain by inductively coupled
690 plasma atomic emission spectrometry. *Journal of the neurological sciences* 146:153–66.

691 Resende RR, Adhikari A, da Costa JL, Lorençon E, Ladeira MS, Guatimosim S, Kihara AH,
692 Ladeira LO. 2010. Influence of spontaneous calcium events on cell-cycle progression in
693 embryonal carcinoma and adult stem cells. *Biochimica et biophysica acta* 1803:246–60.
694 DOI: 10.1016/j.bbamcr.2009.11.008.

695 Riederer P, Sofic E, Rausch WD, Schmidt B, Reynolds GP, Jellinger K, Youdim MB. 1989.
696 Transition metals, ferritin, glutathione, and ascorbic acid in parkinsonian brains. *Journal of*
697 *neurochemistry* 52:515–20.

698 Rosas HD, Chen YI, Doros G, Salat DH, Chen N, Kwong KK, Bush A, Fox J, Hersch SM. 2012.
699 Alterations in brain transition metals in Huntington disease: an evolving and intricate story.
700 *Archives of neurology* 69:887–93. DOI: 10.1001/archneurol.2011.2945.

701 Sanz R, Ferraro GB, Fournier AE. 2015. IgLON cell adhesion molecules are shed from the cell
702 surface of cortical neurons to promote neuronal growth. *The Journal of biological chemistry*
703 290:4330–42. DOI: 10.1074/jbc.M114.628438.

704 Schaarschmidt G, Wegner F, Schwarz SC, Schmidt H, Schwarz J. 2009. Characterization of
705 voltage-gated potassium channels in human neural progenitor cells. *PLoS ONE* 4. DOI:
706 10.1371/journal.pone.0006168.

707 Shin HY, Hong YH, Jang SS, Chae HG, Paek SL, Moon HE, Kim DG, Kim J, Paek SH, Kim SJ.
708 2010. A role of canonical transient receptor potential 5 channel in neuronal differentiation
709 from A2B5 neural progenitor cells. *PloS one* 5:e10359. DOI:
710 10.1371/journal.pone.0010359.

711 Siddappa AJM, Rao RB, Wobken JD, Casperson K, Leibold EA, Connor JR, Georgieff MK.
712 2003. Iron deficiency alters iron regulatory protein and iron transport protein expression in
713 the perinatal rat brain. *Pediatric research* 53:800–7. DOI:
714 10.1203/01.PDR.0000058922.67035.D5.

715 Silvestre DC, Maccioni HJF, Caputto BL. 2009. Content of endoplasmic reticulum and golgi
716 complex membranes positively correlates with the proliferative status of brain cells. *Journal*
717 *of Neuroscience Research* 87:857–865. DOI: 10.1002/jnr.21915.

718 Sîrbulescu RF, Ilieş I, Zupanc GKH. 2015. Matrix metalloproteinase-2 and -9 in the cerebellum
719 of teleost fish: Functional implications for adult neurogenesis. *Molecular and cellular*
720 *neurosciences* 68:9–23. DOI: 10.1016/j.mcn.2015.03.015.

721 Sochacki J, Devalle S, Reis M, Mattos P, Rehen S. 2016. Generation of iPS cell lines from
722 schizophrenia patients using a non-integrative method. *Stem Cell Research*. DOI:
723 10.1016/j.scr.2016.05.015.

724 Sofic E, Riederer P, Heinsen H, Beckmann H, Reynolds GP, Hebenstreit G, Youdim MB. 1988.
725 Increased iron (III) and total iron content in post mortem substantia nigra of parkinsonian
726 brain. *Journal of neural transmission* 74:199–205.

De Souza AS, Fernandes FS, do Carmo M das GT. 2011. Effects of maternal malnutrition and postnatal nutritional rehabilitation on brain fatty acids, learning, and memory. *Nutrition reviews* 69:132–44. DOI: 10.1111/j.1753-4887.2011.00374.x.

Springgate CF, Mildvan AS, Abramson R, Engle JL, Loeb LA. 1973. Escherichia coli deoxyribonucleic acid polymerase I, a zinc metalloenzyme. Nuclear quadrupolar relaxation studies of the role of bound zinc. *The Journal of biological chemistry* 248:5987–93.

Tahmasebi Boroujeni S, Naghdi N, Shahbazi M, Farrokhi A, Bagherzadeh F, Kazemnejad A, Javadian M. 2009. The effect of severe zinc deficiency and zinc supplement on spatial learning and memory. *Biological trace element research* 130:48–61. DOI: 10.1007/s12011-008-8312-7.

Takeda A, Sakurada N, Ando M, Kanno S, Oku N. 2009. Facilitation of zinc influx via AMPA/kainate receptor activation in the hippocampus. *Neurochemistry international* 55:376–82. DOI: 10.1016/j.neuint.2009.04.006.

Tapiero H, Tew KD. 2003. Trace elements in human physiology and pathology: zinc and metallothioneins. *Biomedicine & pharmacotherapy = Biomédecine & pharmacothérapie* 57:399–411.

Tran P V, Carlson ES, Fretham SJB, Georgieff MK. 2008. Early-life iron deficiency anemia alters neurotrophic factor expression and hippocampal neuron differentiation in male rats. *The Journal of nutrition* 138:2495–501. DOI: 10.3945/jn.108.091553.

VanLandingham JW, Levenson CW. 2003. Effect of retinoic acid on ferritin H expression during brain development and neuronal differentiation. *Nutritional neuroscience* 6:39–45. DOI: 10.1080/1028415021000056041.

Wallberg P, Lindberg M, Alsterborg E, Roomans GM, Wróblewski R. 2000. Elemental changes in skin from patients with basal cell carcinoma. *Journal of submicroscopic cytology and pathology* 32:169–73.

Wang H, Wang M, Wang B, Li M, Chen H, Yu X, Yang K, Chai Z, Zhao Y, Feng W. 2012. Immunogold labeling and X-ray fluorescence microscopy reveal enrichment ratios of Cu and Zn, metabolism of APP and amyloid-β plaque formation in a mouse model of Alzheimer's disease. *Metallomics : integrated biometal science* 4:1113–8. DOI: 10.1039/c2mt20056b.

Weissman TA, Riquelme PA, Ivic L, Flint AC, Kriegstein AR. 2004. Calcium waves propagate through radial glial cells and modulate proliferation in the developing neocortex. *Neuron* 43:647–61. DOI: 10.1016/j.neuron.2004.08.015.

Wróblewski R, Chamberlain J, Edström L. 1984. Sodium, phosphorus, sulphur, chlorine and potassium shifts in rat brain during embryonic development. *Brain research* 314:207–15.

762 Wu FY, Huang WJ, Sinclair RB, Powers L. 1992. The structure of the zinc sites of Escherichia
763 coli DNA-dependent RNA polymerase. *The Journal of biological chemistry* 267:25560–7.

764 Yasuda T, Bartlett PF, Adams DJ. 2008. K(ir) and K(v) channels regulate electrical properties
765 and proliferation of adult neural precursor cells. *Molecular and cellular neurosciences*
766 37:284–97. DOI: 10.1016/j.mcn.2007.10.003.

767 Yu X, Jin L, Zhang X, Yu X. 2013. Effects of maternal mild zinc deficiency and zinc
768 supplementation in offspring on spatial memory and hippocampal neuronal ultrastructural
769 changes. *Nutrition (Burbank, Los Angeles County, Calif.)* 29:457–61. DOI:
770 10.1016/j.nut.2012.09.002.

771 Yu X, Ren T, Yu X. 2013. Disruption of calmodulin-dependent protein kinase II α/brain-derived
772 neurotrophic factor (α-CaMKII/BDNF) signalling is associated with zinc deficiency-
773 induced impairments in cognitive and synaptic plasticity. *The British journal of nutrition*
774 110:2194–200. DOI: 10.1017/S0007114513001657.

775

776

777

778

Table 1(on next page)

Trace elements detected in cerebral organoids and its corresponding functions in the brain development

Element	Cellular function	Role in brain development	References
P	Nucleoproteins Phospholipids ATP	Neurogenesis (cellular membrane biogenesis)	(Silvestre, Maccioni & Caputto, 2009)
S	Protein synthesis Cysteine Disulfide bonds	Neurogenesis Neuronal migration (proteoglycans and glycosaminoglycans) Axon guidance	(Inatani et al., 2003; Girós et al., 2007; Maeda, 2015)
K	Protein synthesis RNA synthesis Cell division Transmembrane transport	Resting potential Neurogenesis Neural progenitors' survival	(Lubin & Ennis, 1964; Schaarschmidt et al., 2009)
Ca	Cell signaling Enzymatic cofactor Regulation of gene expression Cell motility	Neurogenesis Neuronal differentiation Release of synaptic vesicles	(Weissman et al., 2004; Shin et al., 2010; Resende et al., 2010; Atlas, 2013)
Fe	DNA synthesis Lipid synthesis Energetic metabolism Metalloproteins	Neurogenesis Neuronal differentiation Monoamine metabolism Modulation of dopaminergic receptors Synaptic maturity Myelin synthesis	(Erikson et al., 2001; VanLandingham & Levenson, 2003; Lozoff & Georgieff, 2006; Tran et al., 2008)
Zn	Protein synthesis DNA synthesis Zinc finger transcription factor Metalloproteins	Neurogenesis Neuronal differentiation Synaptic modulation Dendritic arborization Myelin synthesis	(Liu et al., 1992; Gao et al., 2009; Levenson & Morris, 2011; Morris & Levenson, 2013; Marger, Schubert & Bertrand, 2014)

1

Table 2 (on next page)

Elements' concentrations in cerebral organoids after 30 and 45-days *in vitro* and in adult human cerebral cortex

Values in µg/g, mean±S.D. n=4 for 30-days old cerebral organoids and n=5 for 45-days old cerebral organoids. Values from Rajan et al. (1997) are an average from different regions of cerebrum cortex and S.D. refers to the number of different regions assessed. *Values are significantly different ($p<0.05$) when comparing 30 and 45-days old cerebral organoids.

Concentration (ppm)						
Element	**Present study**		**Sofic et al. (1988)**	**Dexter et al. (1991)**	**Rajan et al. (1997)**	**Rahil-Khazen et al. (2002)**
	30 days	**45 days**				
P	16,142±1,219*	10,286±840*			1,920±256	
S	4,955±350*	4,462±249*				
K	6,120±1,745	3,951±422			3,180±306	
Ca	192±157	286±43			175±6	
Fe	84±61	87±37	28±5.4	58.9	49±7.5	50.2
Zn	129±6*	101±2*		31.25±3.	12.7±6	11.8

1

Table 3(on next page)

Pearson’s correlation coefficients of spatial associations between trace elements in cerebral organoids

The values correspond to the average of at least four different samples and S.D..

1

30 days-old organoids (n=4)					
	S	**K**	**Ca**	**Fe**	**Zn**
P	0.74(0.25)	0.75(0.2)	0.21(0.3)	0.42(0.3)	0.89(0.004)
S		0.87(0.02)	0.31(0.3)	0.42(0.3)	-
K			0.08(0.3)	0.18(0.3)	0.77(0.04)
Ca				0.21(0.3)	0.28(0.3)
Fe					0.56(0.3)

45 days-old organoids (n=5)					
	S	**K**	**Ca**	**Fe**	**Zn**
P	0.89(0.01)	0.86(0.03)	0.73(0.03)	0.55(0.25)	0.84(0.05)
S		0.89(0.04)	0.82(0.07)	0.56(0.25)	0.78(0.09)
K			0.80(0.05)	0.56(0.27)	0.82(0.03)
Ca				0.53(0.16)	0.63(0.13)
Fe					0.55(0.24)

2

Figure 1

Cerebral organoids derived from human embryonic stem cells

Fig 1. Cerebral organoids derived from human embryonic stem cells. (A) Sequential steps involved in generation of cerebral organoids from human pluripotent stem cells. (B) Spheroid cerebral organoids of 45-days old presenting smooth texture and homogeneous coloring. (C and C') Microphotography of a 30-days old organoid in detail with different hues according to different cell layers. (D) Along the differentiation process, organoids' diameter doubled between days 7 and 15 in culture and quintupled after 45 days. The graph represents mean ± S.D. n=107 for 7-days old organoids, n=90 for 15-days old organoids, n=56 for 30-days old organoids, n=18 for 45-days old organoids. ***p < 0.0001 for 7-days old versus 15, 30 and 45-days old organoids. Cerebral organoids were obtained from two independent assays. Scale bars: B = 1 mm, C = 125 µm and C' = 25 µm.

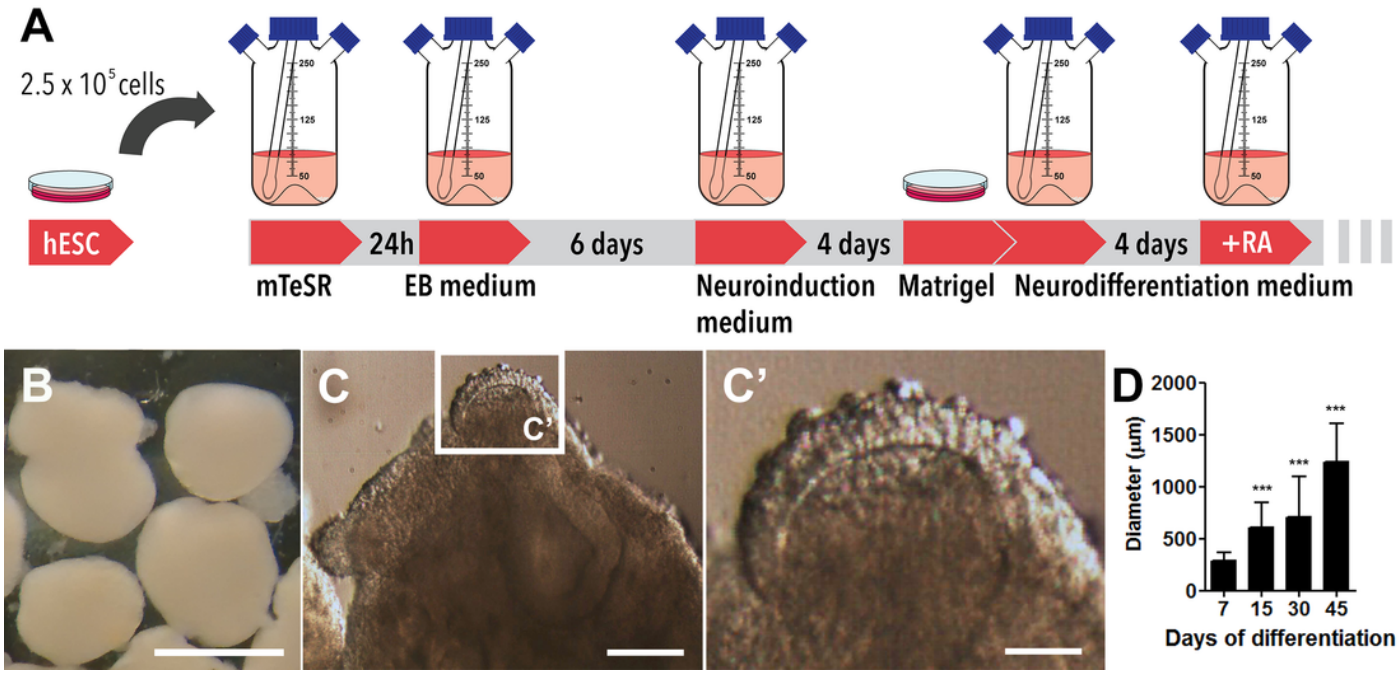

Figure 2

The cytoarchiteture of cerebral organoids after 30 and 45 days in culture

Fig 2: The cytoarchiteture of cerebral organoids after 30 and 45 days in culture. (A) Within 30 days of differentiation, cerebral organoids formed large cavities similar to ventricles. (B) After 45 days of differentiation, the ventricules became significantly smaller. In A and B, images of H&E staining. (C) Ventricles measurements showed a reduction in ventricle per organoid area ratio. The graph represents mean ± S.D. n=11 for ventricles of 30-days old organoids and n=31 for ventricles of 45-days old organoids, *$p < 0.05$. Cerebral organoids were obtained from two independent assays. Scale bars: A and B = 500 µm, small inserts = 200 µm.

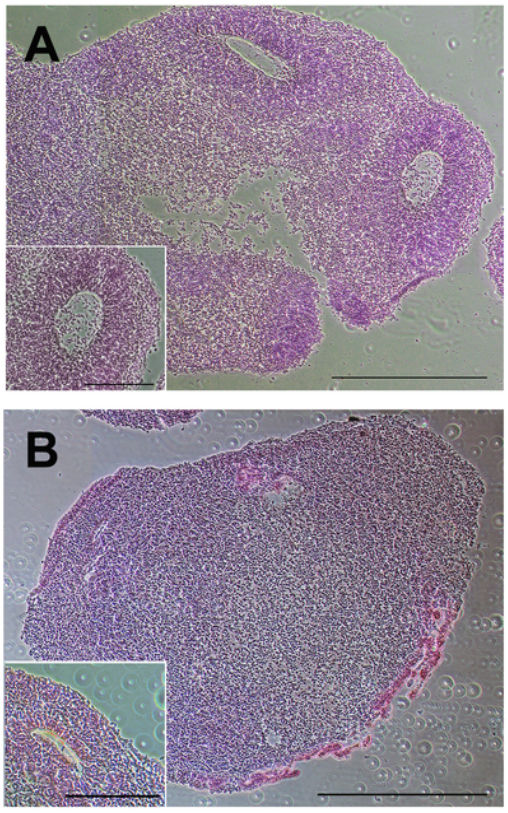
A
B

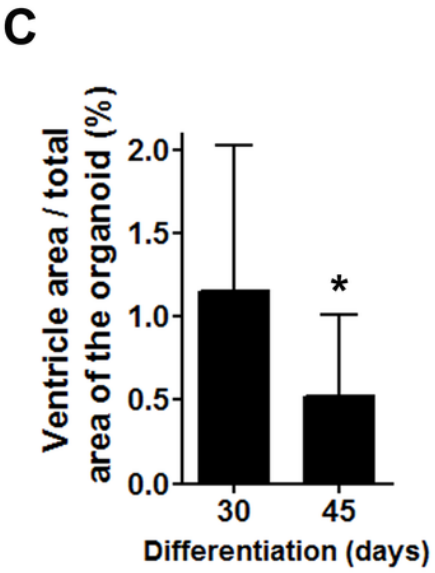
C
Ventricle area / total area of the organoid (%)
2.0
1.5
1.0
0.5
0.0
*
30
45
Differentiation (days)

Figure 3

Cell types and neuronal structures in cerebral organoid after 30 days in culture

Fig 3: Cell types and neuronal structures in cerebral organoid after 30 days in culture. (A) Positive cells for the intermediate filament nestin were present all over the cerebral organoids. (B) The luminal surface was populated by mitotic cells (phospho histone H3, PH3), (C) along with apical progenitors (PAX6) that delineated the ventricular zone. (D) TBR2 was also expressed in the ventricular zone and formed an adjacent layer of intermediate progenitors, the subventricular zone. (C and D) Tangentially migrating neurons (β-tubulin III and MAP2) established the pre-plate. Scale bars: A, B = 100 µm; C = 50 µm; D = 100 µm.

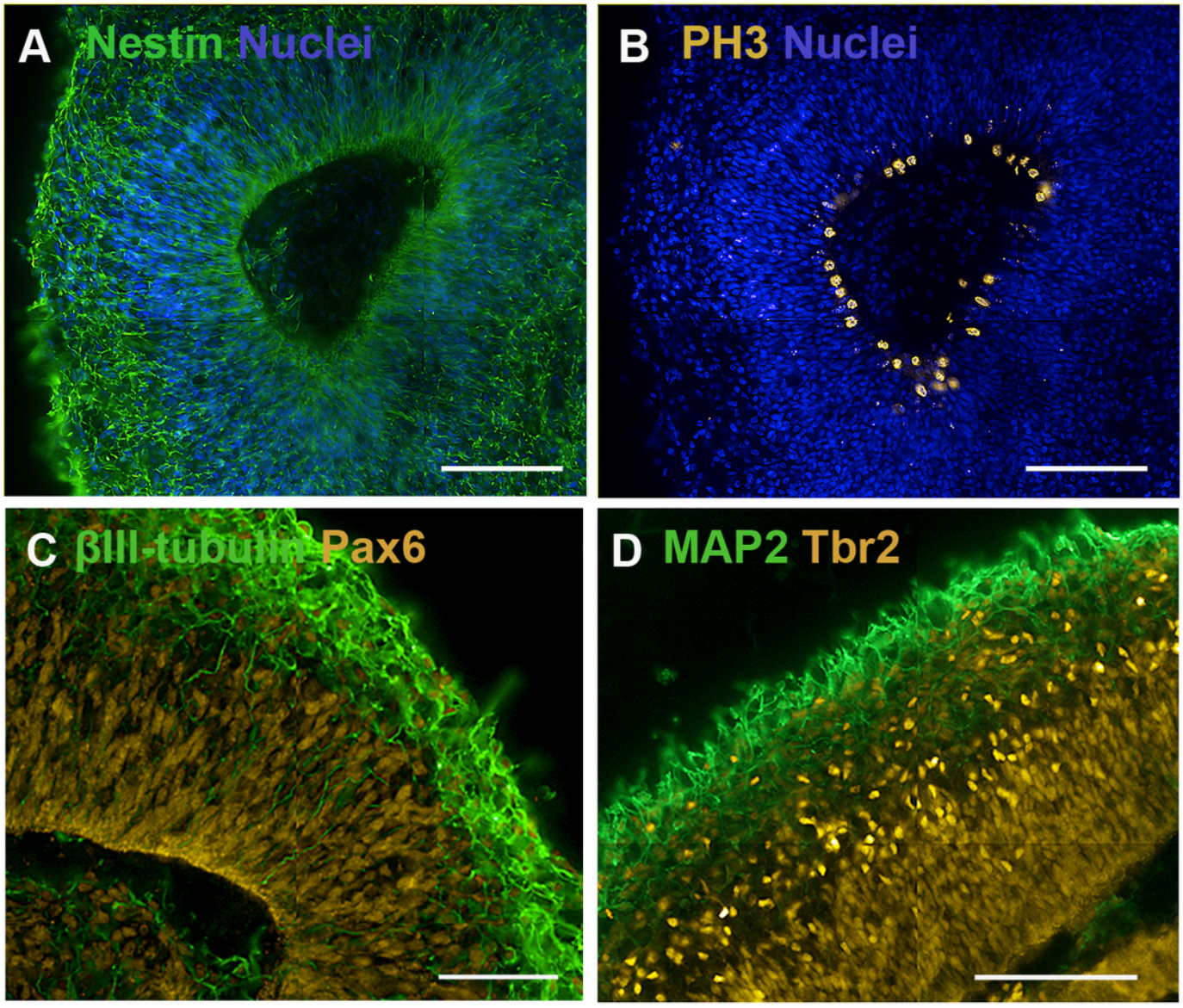
A Nestin Nuclei
B PH3 Nuclei
C βIII-tubulin Pax6
D MAP2 Tbr2

Figure 4

Cell types and neuronal structures in cerebral organoid after 45 days in culture

Fig 4: Cell types and neuronal structures in cerebral organoid after 45 days in culture. (A) MAP2 positive cells were spread all over the cerebral organoids, while cells expressing the enzyme to synthetize GABA (GAD67, B) or the neurotransmitter glutamate (C) were also present. (D) Synaptic markers such as synaptophysin and PSD95 were also observed. Scale bars: A = 100 µm; B, C and D = 50 µm.

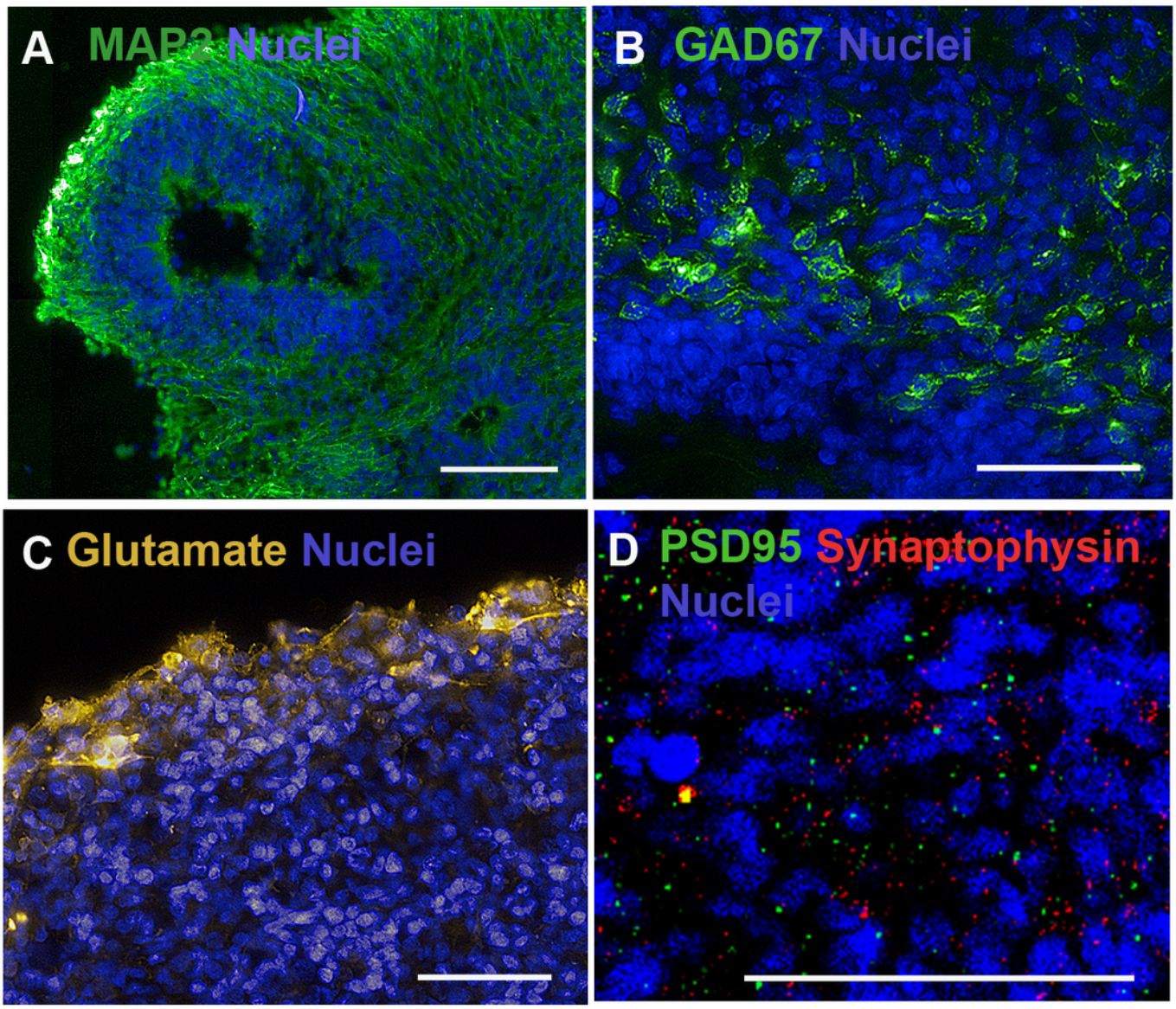

Figure 5

Quantification of proliferative and neuronal differentiation markers

Fig 5: Quantification of proliferative and neuronal differentiation markers. (A) Comparing 30 to 45-days old cerebral organoids, a progressive reduction in the number of PH3 positive cells indicated a reduced mitotic activity. In accordance with a switch from a self-renewal to a neuronal differentiation phase of neuronal progenitors, the neuronal population was expanded (B) as well as neurons producing GABA (C) or cells producing glutamate (D). Graphs are represented as mean ± S.D. For 30-days old and 45-days old organoids: PH3 positive cells, n=3 and n=5; MAP2 area, n=4 and n=6; GAD67 positive cells, n=2 and n=4; glutamate fluorescence intensity, n=6 and n=7, respectively, *$p<0.05$.

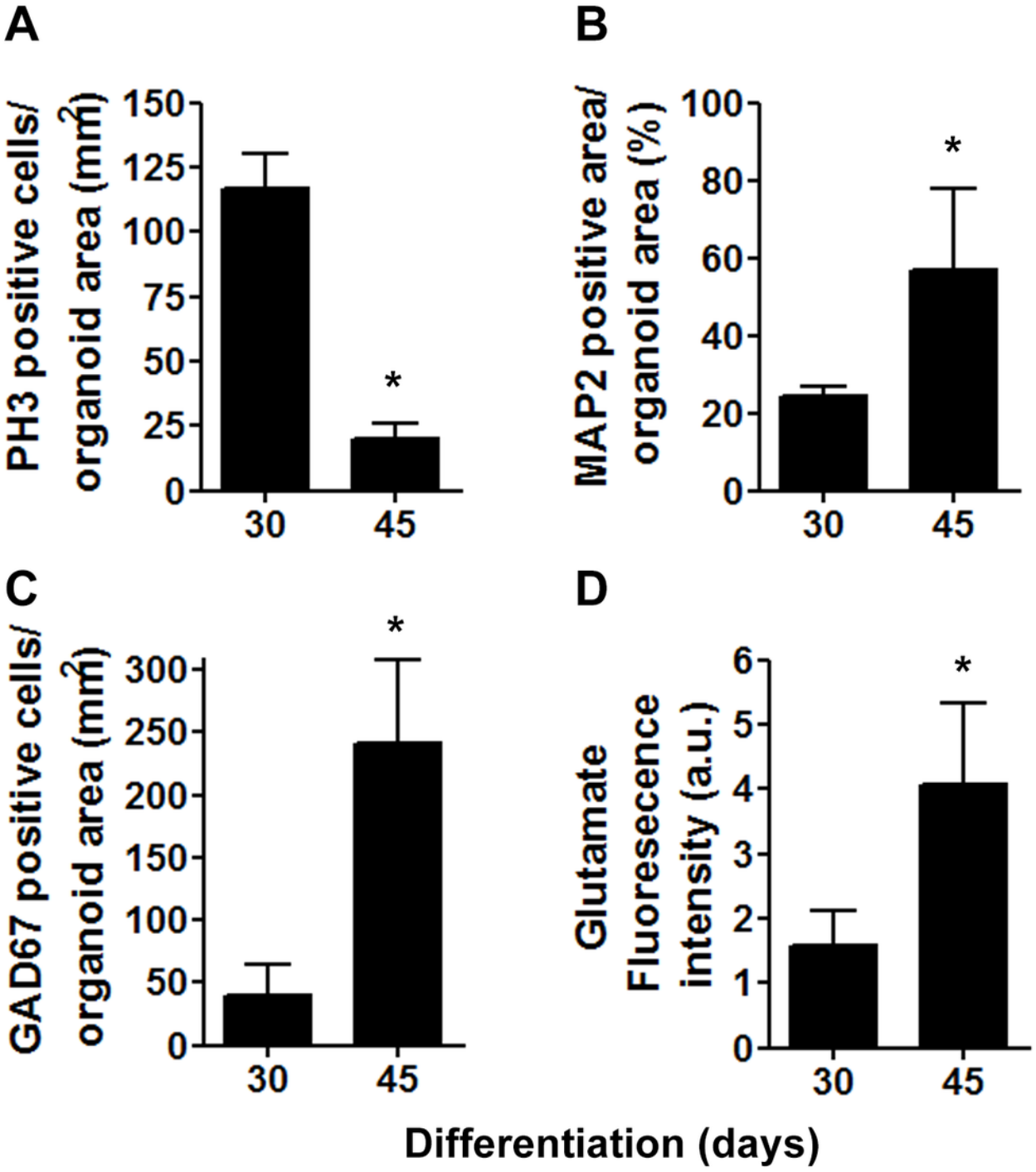
A
PH3 positive cells/ organoid area (mm2)
150
125
100
75
50
25
0
*
30
45
B
MAP2 positive area/ organoid area (%)
100
80
60
40
20
0
*
30
45
C
GAD67 positive cells/ organoid area (mm2)
300
250
200
150
100
50
0
*
30
45
D
Glutamate Fluoresecence intensity (a.u.)
6
5
4
3
2
1
0
*
30
45
Differentiation (days)

Figure 6(on next page)

Atomic distribution in cerebral organoids

Fig 6: Atomic distribution in cerebral organoids. Representative heat maps of 30 and 45-days old cerebral organoids. The patterns of elements distribution were useful to indicate diffusion throughout organoids's extension (S, Ca and Fe) or higher levels in the organoids' border (P and Zn).